POLITECNICO DI TORINO
Repository ISTITUZIONALE

Investigation of collimating and focusing lenses impact on laser diode stack beam parameter product

Original
Investigation of collimating and focusing lenses impact on laser diode stack beam parameter product / Yu, H., Liu, Y.u., Braglia, A., Rossi, G., Perrone, G.. - In: APPLIED OPTICS. - ISSN 1559-128X. - STAMPA. - 54:34(2015), pp. 10240-10248. [10.1364/AO.54.010240]

Availability:
This version is available at: 11583/2627039 since: 2015-12-29T12:06:16Z

Publisher:
Optical Society of America

Published
DOI:10.1364/AO.54.010240

Terms of use:

This article is made available under terms and conditions as specified in the corresponding bibliographic description in the repository

Publisher copyright
Optica Publishing Group (formely OSA) postprint/Author's Accepted Manuscript

"© 2015 Optica Publishing Group. One print or electronic copy may be made for personal use only. Systematic reproduction and distribution, duplication of any material in this paper for a fee or for commercial purposes, or modifications of the content of this paper are prohibited."

(Article begins on next page)

23 June 2026

Investigation of collimating and focusing lenses impact on laser diode stack beam parameter product

HAO YU[1], YU LIU[1], ANDREA BRAGLIA[1,2], GIAMMARCO ROSSI[2], AND GUIDO PERRONE[1,*]

[1] Department of Electronics and Telecommunications, Politecnico di Torino, C.so Duca degli Abruzzi 24, I-10129 Torino, Italy
[2] OPI Photonics S.R.L., 3 V. Conte Rosso 3, I-10121 Torino, Italy
[*] Corresponding author: guido.perrone@polito.it

Compiled October 29, 2015

The paper presents a new expression for the determination of the Beam Parameter Product (BPP) of a multi-emitter laser diode module made by stacking several single emitter chips. The proposed formula takes into account the effect of collimating and focusing lenses, and has been validated experimentally, obtaining an excellent agreement between theoretical expectations and measurements. A practical application to optimize the lenses configuration for the design of a fiber-coupled multi-emitter module is also reported. © 2015 Optical Society of America

OCIS codes: *(080.2740) Geometric optical design; (140.2010) Diode laser arrays; (140.3295) Laser beam characterization; (140.3298) Laser beam combining; (140.3325) Laser coupling.*

http://dx.doi.org/10.1364/ao.XX.XXXXXX

1. INTRODUCTION

The combination of multi-emitter semiconductor laser chips or mini-bars [1, 2] is emerging as the most reliable and cost-effective technological path for the development of kilowatt range diode based laser sources, both for direct applications [3] (e.g. welding, brazing, surface treatment, cladding, etc.) and for pumping high power fiber lasers [4, 5].

In particular, the direct use of diodes for material processing in industrial applications is currently attracting a large interest because it does not imply additional power penalties due to the limited efficiency of the pump absorption - signal emission mechanism of diode pumped lasers. These applications, however, require a good compromise between signal power and beam quality, which therefore must be carefully preserved in the combination of the individual laser sources.

A multi-emitter high power module is composed of a number of single emitting chips or bars, whose output beams are combined exploiting three different approaches, namely spatial (also known as "beam stacking"), polarization, and wavelength multiplexing. Spatial multiplexing is practically unavoidable and it is also the technique most affecting the beam quality degradation. It is realized using an optical system that arranges side by side the beams and then focuses them, often in a multi-mode fiber (at least for fiber coupled modules). The sketch of a typical multi-emitter module configuration that makes use of spatial multiplexing is shown in Fig. 1 [6].

Beam quality plays an important role also when the multi-emitter module is used for pumping another laser, such as in the case of fiber lasers (an example is in Fig. 2), since the beam quality determines the number of modules that can be coupled to an active fiber of given size and numerical aperture. This because the power of fiber lasers increases with the total pump power, which in turn is proportional to the number of chips that can be coupled inside a multi-emitter module and then to the number of modules that can be coupled into the fiber, and this depends on the beam quality.

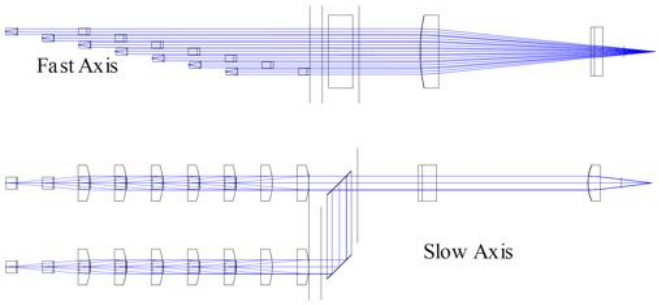

Fig. 1. Typical configuration of a multi-emitter laser diode module that makes use of spatial multiplexing.

The key parameter to evaluate the beam quality of high power lasers is the "Beam-Parameter-Product" (BPP), which for Gaussian beams is defined as the product of the beam radius measured at the waist and the beam divergence angle measured in the far field; for non-Gaussian beams, second order moments are used to define the beam radius and the divergence. The

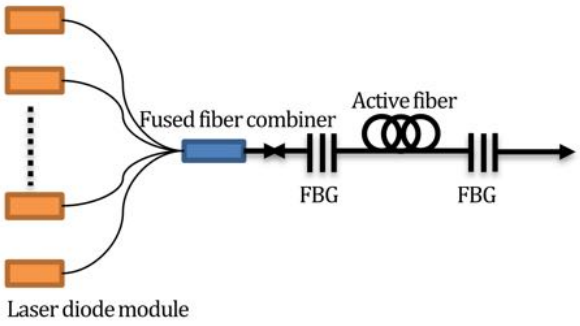

Fig. 2. Typical architecture of high power fiber lasers pumped from one end by a combination of multi-emitter laser diode modules.

smallest possible BPP is for diffraction-limited Gaussian beams, and the higher the beam quality, the lower the BPP. Moreover, the BPP is an optical invariant, so it cannot be only degraded by passive optical systems. Therefore, investigating how the beam quality of laser diode chips modifies when combined into stacks is important for at least two reasons: i) determine the power loss due to the mismatch with the BPP of the optical device into which the stacked beam is coupled (most often a fiber, realizing the so called fiber-pigtailed modules; so in the following a fiber will be assumed as this optical device); ii) optimize the configuration of the laser diode stack by maximizing the number of chips that can be combined given the output fiber characteristics.

Semiconductor laser diodes emit a beam with very different properties along the two main directions, known as "Slow" and "Fast" Axes (SA and FA, respectively), and various criteria have been followed to provide a single parameter able to characterize the beam quality. One of the most used relations is [7]

$$\mathrm{BPP_{dia}} = (\mathrm{BPP_{slow}^2} + \mathrm{BPP_{fast}^2})^{1/2}, \quad \textbf{(1)}$$

where $\mathrm{BPP_{dia}}$ is the diagonal BPP of a laser diode stack, and $\mathrm{BPP_{fast}}$ and $\mathrm{BPP_{slow}}$ denote the BPP along fast axis (FA) and slow axis (SA) direction, respectively. Another common definition is [8]

$$\mathrm{BPP_{dia}} = \mathrm{BPP_{slow}} + \mathrm{BPP_{fast}}. \quad \textbf{(2)}$$

Previous literature states that for efficient fiber coupling $\mathrm{BPP_{dia}}$ has to be smaller than the BPP of the fiber ($\mathrm{BPP_{fiber}}$) into which the beam has to be coupled, but to the best of our knowledge the proof is found in published literature only for Eq. 2 [8]. In our work, we found that Eq. 2 is a special case of our new expression for the BPP of a laser diode stack. This value sets the minimum BPP of laser diode stacks and is critically dependent on the choice of the optical components used to collimate and focus the single beams, namely the Fast Axis Collimator (FAC), the Slow Axis Collimator (SAC), the FA focusing lens and the SA focusing lens. In the remaining of the paper we describe a model for calculating the minimal diagonal BPP of laser diode stack and for evaluating the best combination of FAC, SAC, FA focusing lens and SA focusing lens; then we provide an experimental validation of such model.

2. MODEL DESCRIPTION

For sake of simplicity, but without losing generality, we assume that:

1. The beam emitted by the single laser diode chip has a rectangular shape, as depicted in Fig. 3.

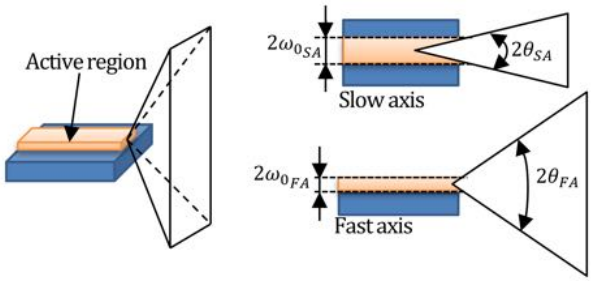

Fig. 3. Simplified laser diode radiation model.

2. The beam divergence after collimation is negligible (i.e., the beam radii along the fast and slow directions are practically constants with propagation); this is reasonable because well-collimated beams have extremely small divergences, so that after the propagation paths typical of module packages the variation of beam size is almost below measurement capabilities. For example, considering a common 915 nm laser chip with $1/e^2$ intensity beam waist radius of 0.8 µm and divergence of 400 mrad (23 degrees) in the FA direction and, respectively, of 47 µm and 115 mrad (6.5 degrees) in the SA direction, the divergence becomes 1.3 mrad in the FA direction and 3.9 mrad in the SA directions after respective collimation with a FAC having an Effective Focal Length (EFL) of 0.6 mm and a SAC having EFL of 12 mm.

3. All the beams emitted by the single laser chips are incoherent with respect to each other and thus there is no interference.

4. All the lenses are aberration-free.

5. Laser diodes are arranged at a fixed interval along the FA as shown in Fig. 4, and placed linearly along the SA as depicted in Fig. 5.

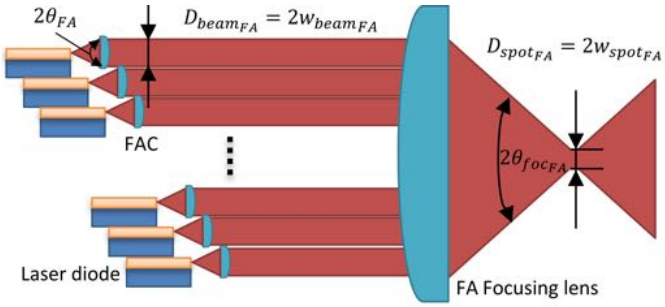

Fig. 4. N_{FA} laser diodes arrangement along the FA; besides for the vertical stacking, the picture shows also a longitudinal offset, which is necessary for the practical implementation of the multi-emitters but does not impact on the model derivation.

It is well known that the beams emitted from laser diodes are not exactly Gaussian shaped; nevertheless they can be analyzed with the same formalism by introducing the M^2 correction factor [9]. Let's consider the example of Fig. 4. Given that the EFL

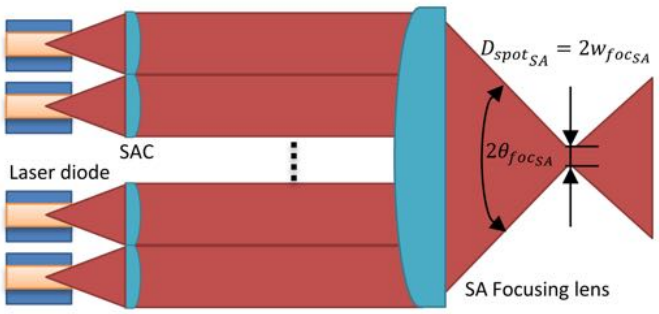

Fig. 5. N_{SA} laser diodes arrangement along the SA.

of the collimating lens is usually much larger than the Rayleigh length, the beam radius after the FAC can be approximated as

$$w_{\text{beam}_{\text{FA}}} \approx \frac{M^2_{\text{FA}}\lambda}{\pi w_{0_{\text{FA}}}} f_{\text{FAC}} = \theta_{\text{FA}} f_{\text{FAC}}, \tag{3}$$

where f_{FAC} is the EFL of the FAC, and M^2_{FA} and θ_{FA} are the M^2 factor and the beam divergence along the FA, respectively.

After being collimated, the beam passes through a focusing lens and concentrates at the focal plane; the spot size at this position is [10]

$$w_{\text{spot}_{\text{FA}}} = \frac{M^2_{\text{FA}}\lambda}{\pi w_{\text{beam}_{\text{FA}}}} f_{\text{foc}_{\text{FA}}}, \tag{4}$$

where $w_{\text{beam}_{\text{FA}}}$ is the beam waist radius at the lens and $f_{\text{foc}_{\text{FA}}}$ is the EFL of the FA focusing lens.

Given the assumption that the divergence of the collimated beam is negligible and the beam waist radius is constant after collimation, by substituting Eq. 3 into Eq. 4 we obtain

$$w_{\text{spot}_{\text{FA}}} = \frac{\text{BPP}_{\text{FA}}}{\theta_{\text{FA}}} \frac{f_{\text{foc}_{\text{FA}}}}{f_{\text{FAC}}}, \tag{5}$$

where we used the expression

$$\text{BPP}_{\text{FA}} = \frac{M^2_{\text{FA}}\lambda}{\pi}.$$

The divergence of the focused beam is

$$\theta_{\text{foc}_{\text{FA}}} = \frac{w_{\text{beam}_{\text{FA}}}}{f_{\text{foc}_{\text{FA}}}} = \frac{\theta_{\text{FA}} f_{\text{FAC}}}{f_{\text{foc}_{\text{FA}}}}. \tag{6}$$

In the case of multi-emitters with N laser diodes distributed vertically as depicted in Fig. 4, the combined collimated beams can be seen as a unique beam of width equal to $N \cdot w_{\text{beam}_{\text{FA}}}$ but the spot waist radius remains constant. Hence the divergence of the focused beam changes to

$$\theta_{\text{foc}_{\text{FA}}} = N \frac{w_{\text{beam}_{\text{FA}}}}{f_{\text{foc}_{\text{FA}}}} = N \frac{\theta_{\text{FA}} f_{\text{FAC}}}{f_{\text{foc}_{\text{FA}}}}. \tag{7}$$

As evident from Fig. 4, each beam can be truncated by nearby lenses and possibly limited by the focusing lens clear aperture, if this is not large enough. Consequently, some power is lost by the truncation, but this is not considered in the model since the loss should be less than few percents (typically $< 7\%$) under correct design and choice of the lenses. As mentioned before, at the focal plane the spot size of a N diode combined beam is the same as the spot size of a single diode. This can be proved by considering for instance 2 incident beams of amplitude $A(x)$; the expression of the combination of the 2 beams entering the lens is

$$A_{\text{all}}(x) = A(x)\exp(j\phi_1) + A(x + x_{\text{offset}})\exp(j\phi_2), \tag{8}$$

being x_{offset} the distance between the two diodes, $A(x)$ the amplitude of a single beam at the entrance of the focusing lens, and ϕ_1 and ϕ_2 the phases of two beams, respectively.

The amplitude at the focal plane is the Fourier Transform of Eq. 8, which is

$$A'_{\text{all}}(f_x) = A'(f_x)[\exp(j\phi_1) + \exp(-2\pi j x_{\text{offset}} f_x)\exp(j\phi_2)], \tag{9}$$

where $A'(x)$ is the Fourier Transform of a single beam at the focal plane.

The intensity at the focal plane becomes

$$\begin{aligned}|A'_{\text{all}}(f_x)|^2 =& |A'(f_x)|^2[2 + \exp(-2\pi j x_{\text{offset}} f_x - j\triangle\phi) + \\ & \exp(2\pi j x_{\text{offset}} f_x + j\triangle\phi)],\end{aligned} \tag{10}$$

where f_x is the spatial frequency, and $\triangle\phi$ is the phase difference between ϕ_1 and ϕ_2.

Since the two beams are incoherent, the phase difference $\triangle\phi$ is random and Eq. 10 reduces to $|A'_{\text{all}}(f_x)|^2 = 2|A'(f_x)|^2$. Extending the result to N beams, the resulting intensity is

$$\begin{aligned}|A'_{\text{all}}(f_x)|^2 =& |A'(f_x)|^2 \left[N + \sum_{\text{m}=0}^{\text{N}-1} \exp(-2m\pi j x_{\text{offset}} f_x) \cdot \right. \\ & \left. \sum_{\text{n}=0,\text{n}!=\text{m}}^{\text{N}-1} \exp(2n\pi j x_{\text{offset}} f_x) \exp\left(j(\phi_{\text{n}} - \phi_{\text{m}})\right) \right].\end{aligned} \tag{11}$$

Hence, for N incoherent beams the intensity at the focal plane is $N|A'(f_x)|^2$, and thus the spot size of N beams is identical to the spot of a single beam, the difference being only in the intensity.

Similar reasoning applies along the SA; then the result can be further extended to the actual case where the combination is of two dimensional beams with different spot sizes in the two main directions. Assuming that there are N_{FA} laser diodes along the FA direction and N_{SA} along the SA direction, the beam waist radius of this stack at the focal plane can be expressed as

$$w_{\text{dia}} = \sqrt{\left(\frac{\text{BPP}_{\text{FA}}}{\theta_{\text{FA}}} \frac{f_{\text{foc}_{\text{FA}}}}{f_{\text{FAC}}}\right)^2 + \left(\frac{\text{BPP}_{\text{SA}}}{\theta_{\text{SA}}} \frac{f_{\text{foc}_{\text{SA}}}}{f_{\text{SAC}}}\right)^2}, \tag{12}$$

where BPP_{FA}, θ_{FA}, and $f_{\text{foc}_{\text{FA}}}$ are, respectively, the BPP, the beam divergence and the EFL of the focusing lens along the FA direction; similarly for BPP_{SA}, θ_{SA}, and $f_{\text{foc}_{\text{SA}}}$ along the SA direction. Then, f_{FAC} and f_{SAC} are the EFL of the collimating lens along the two FA and SA directions.

The divergence of the the focused beam is

$$\theta_{\text{dia}} = \sqrt{\left(N_{\text{FA}} \frac{\theta_{\text{FA}} f_{\text{FAC}}}{f_{\text{foc}_{\text{FA}}}}\right)^2 + \left(N_{\text{SA}} \frac{\theta_{\text{SA}} f_{\text{SAC}}}{f_{\text{foc}_{\text{SA}}}}\right)^2}. \tag{13}$$

By multiplying Eq. 12 and Eq. 13, the BPP of the combined beam ("diagonal") can be obtained

$$\begin{aligned}\mathrm{BPP}_{\mathrm{dia}} &= \sqrt{\left(\frac{\mathrm{BPP}_{\mathrm{FA}}}{\theta_{\mathrm{FA}}}\frac{f_{\mathrm{foc}_{\mathrm{FA}}}}{f_{\mathrm{FAC}}}\right)^2+\left(\frac{\mathrm{BPP}_{\mathrm{SA}}}{\theta_{\mathrm{SA}}}\frac{f_{\mathrm{foc}_{\mathrm{SA}}}}{f_{\mathrm{SAC}}}\right)^2}\cdot \\ &\sqrt{\left(N_{\mathrm{FA}}\frac{\theta_{\mathrm{FA}}f_{\mathrm{FAC}}}{f_{\mathrm{foc}_{\mathrm{FA}}}}\right)^2+\left(N_{\mathrm{SA}}\frac{\theta_{\mathrm{SA}}f_{\mathrm{SAC}}}{f_{\mathrm{foc}_{\mathrm{SA}}}}\right)^2} \\ &= \left[(N_{\mathrm{FA}}\mathrm{BPP}_{\mathrm{FA}})^2+\left(N_{\mathrm{FA}}\mathrm{BPP}_{\mathrm{SA}}\frac{\theta_{\mathrm{FA}}f_{\mathrm{FAC}}f_{\mathrm{foc}_{\mathrm{SA}}}}{\theta_{\mathrm{SA}}f_{\mathrm{SAC}}f_{\mathrm{foc}_{\mathrm{FA}}}}\right)^2+\right. \\ &\left.(N_{\mathrm{SA}}\mathrm{BPP}_{\mathrm{SA}})^2+\left(N_{\mathrm{SA}}\mathrm{BPP}_{\mathrm{FA}}\frac{\theta_{\mathrm{SA}}f_{\mathrm{SAC}}f_{\mathrm{foc}_{\mathrm{FA}}}}{\theta_{\mathrm{FA}}f_{\mathrm{FAC}}f_{\mathrm{foc}_{\mathrm{SA}}}}\right)^2\right]^{1/2}.\end{aligned} \tag{14}$$

Let:

$$\begin{aligned}A &= \left(N_{\mathrm{FA}}\mathrm{BPP}_{\mathrm{SA}}\frac{\theta_{\mathrm{FA}}f_{\mathrm{FAC}}}{\theta_{\mathrm{SA}}f_{\mathrm{SAC}}}\right)^2 \\ B &= \left(N_{\mathrm{SA}}\mathrm{BPP}_{\mathrm{FA}}\frac{\theta_{\mathrm{SA}}f_{\mathrm{SAC}}}{\theta_{\mathrm{FA}}f_{\mathrm{FAC}}}\right)^2 \\ c &= \left(\frac{f_{\mathrm{foc}_{\mathrm{SA}}}}{f_{\mathrm{foc}_{\mathrm{FA}}}}\right)^2 \\ g(c) &= \mathrm{BPP}_{\mathrm{dia}}^2.\end{aligned}$$

Squaring both sides of Eq. 14 and then substituting A, B and c in it we obtain

$$\begin{aligned}g(c) &= \mathrm{BPP}_{\mathrm{dia}}^2 \\ &= (N_{\mathrm{FA}}\mathrm{BPP}_{\mathrm{FA}})^2+(N_{\mathrm{SA}}\mathrm{BPP}_{\mathrm{SA}})^2+Ac+B\frac{1}{c}.\end{aligned} \tag{15}$$

It is easy to show that

$$\begin{aligned}g(c) &\geqslant (N_{\mathrm{FA}}\mathrm{BPP}_{\mathrm{FA}})^2+(N_{\mathrm{SA}}\mathrm{BPP}_{\mathrm{SA}})^2+2\sqrt{AB} \\ &= (N_{\mathrm{FA}}\mathrm{BPP}_{\mathrm{FA}}+N_{\mathrm{SA}}\mathrm{BPP}_{\mathrm{SA}})^2,\end{aligned}$$

where the equality holds if and only if

$$c = \left(\frac{f_{\mathrm{foc}_{\mathrm{SA}}}}{f_{\mathrm{foc}_{\mathrm{FA}}}}\right)^2 = \sqrt{B/A}. \tag{16}$$

Therefore the minimum of $g(c)$ is $(N_{\mathrm{FA}}\mathrm{BPP}_{\mathrm{FA}}+N_{\mathrm{SA}}\mathrm{BPP}_{\mathrm{SA}})^2$, which for $N_{\mathrm{FA}}=N_{\mathrm{SA}}=1$ gives Eq. 2.

To summarize, we have derived the general expression for the diagonal (or combined) BPP of a $N_{\mathrm{FA}}\times N_{\mathrm{SA}}$ laser diodes stack and this expression can be then used to properly design the optics inside the module and thus optimize its performance. This will be shown in the next section.

3. MAXIMIZING BRILLIANCE

One key indicator of multi-emitter performance is its brilliance, which can be maximized for a given output delivery fiber by coupling into it as much power as possible. Usually laser diode characteristics (active region size, and spot sizes and divergence angles in the FA and SA directions), fiber parameters (core diameter and numerical aperture), and FAC and SAC focal lengths are given; thus the variables on which we can play to maximize the performance are N_{FA}, N_{SA}, $f_{\mathrm{foc}_{\mathrm{FA}}}$ and $f_{\mathrm{foc}_{\mathrm{SA}}}$.

The fiber, a largely multi-mode one, limits the maximum number of laser chips in the multi-emitter by forcing two constrains:

1. The core radius imposes $w_{\mathrm{dia}}\leqslant w_{\mathrm{fiber}}$.
2. The Numerical Aperture (NA) imposes $\theta_{\mathrm{dia}}\leqslant \arcsin(NA)\approx NA$.

Since high power diodes are designed with a large active region along the SA to keep facet power density below a safe limit and avoid catastrophic optical mirror damage, the $\mathrm{BPP}_{\mathrm{SA}}$ is much worse than the $\mathrm{BPP}_{\mathrm{FA}}$ and usually it is impossible to arrange more than one laser diode along the SA; therefore in the following we consider mainly the $N_{\mathrm{SA}}=1$ case. Fig. 5 provides a simple pictorial demonstration: more than one laser diode is probably arranged along the SA if $2\mathrm{BPP}_{\mathrm{SA}}\leqslant\mathrm{BPP}_{\mathrm{fiber}}$, otherwise not all the power can be fully coupled. For instance, if a laser diode has $\mathrm{BPP}_{\mathrm{FA}}$=0.32 mm mrad and $\mathrm{BPP}_{\mathrm{SA}}$=5.4 mm mrad, it is possible to couple a 7 (along the FA) × 2 (along the SA) array into a 200 µm diameter core and 0.22 NA fiber, as shown in Fig. 6. However, for a 100 µm diameter core and 0.22 NA fiber, it is impossible to fully couple that array into the fiber.

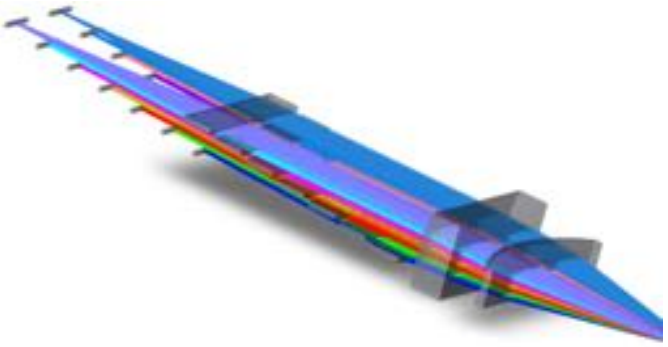

Fig. 6. Model of 7 × 2 laser diode stack with collimating and focusing lenses.

Given N_{SA}, from the previously derived relations, the maximum number of laser diodes along the FA is

$$N_{\mathrm{FA}} = \mathrm{floor}\left[(\mathrm{BPP}_{\mathrm{fiber}}-N_{\mathrm{SA}}\mathrm{BPP}_{\mathrm{SA}})/\mathrm{BPP}_{\mathrm{FA}}\right]. \tag{17}$$

This value represents an upper bound, and it is a necessary but not sufficient condition. Therefore we have to enforce also the second constrain posed by the output fiber: $\theta_{\mathrm{dia}}\leqslant NA$. This condition turns into:

$$f_{\mathrm{foc}_{\mathrm{FA}}}\geqslant\frac{\theta_{\mathrm{FA}}f_{\mathrm{FAC}}}{NA}\sqrt{N_{\mathrm{FA}}^2+\frac{N_{\mathrm{FA}}N_{\mathrm{SA}}BPP_{\mathrm{SA}}}{BPP_{\mathrm{FA}}}}. \tag{18}$$

The maximum of brilliance is achieved when the equality in Eq. 18 holds. Recalling then Eq. 16, the optimal case is for:

$$f_{\mathrm{foc}_{\mathrm{SA}}} = f_{\mathrm{foc}_{\mathrm{FA}}}\sqrt[4]{B/A}. \tag{19}$$

Eq. 18 and Eq. 19 give an insight of the impact the focusing lenses have in minimizing $\mathrm{BPP}_{\mathrm{dia}}$ by balancing $\mathrm{BPP}_{\mathrm{FA}}$ and $\mathrm{BPP}_{\mathrm{SA}}$.

4. EXPERIMENTAL SETUP

The design rules outlined in the previous section have been verified experimentally using a commercial laser chip, whose nominal parameters are reported in Tab. 1 [11]. The laser chip has been used at 8 A current, corresponding to approximatively 8 W of emitted power at a temperature of about 30°C.

Prior to experimentally validate the diode stacking limits, near and far field measurements of the laser chip have been taken using well-known imaging techniques to evaluate the parameters needed in the model.

Table 1. Main data of the commercial laser chip used for the experimental validation of the developed model.

Quantity	Value
CW Output Power (W)	9
Center Wavelength (nm)	915 ± 10
FA FWHM Beam divergence (deg)	23
SA FWHM Beam divergence (deg)	8
SA Emitter Width (µm)	90

A. Near-field Measurements

The experimental setup to measure the near field of a laser diode is schematically shown in Fig. 7. The beam is collimated by the F1 lens, sampled using a wedge prism, further attenuated by a set of Neutral Density (ND) filters, focused by the F2 lens, and imaged onto a CCD camera.

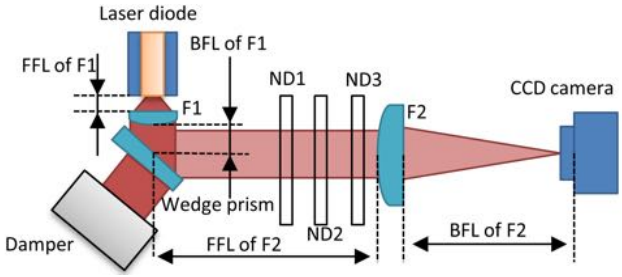

Fig. 7. Near-field measurement setup.

The obtained near-field image is reported in Fig. 8. From this image, the size of the active region w_0 along one of the two axes can be calculated considering that

$$w_0 = \frac{f_1}{f_2} d_{\text{mea}}, \tag{20}$$

where f_1 is the EFL of F1, f_2 is the EFL of F2 and d_{mea} is the distance measured on the image; from an image area of 0.0528 $\times$ 3.0096 mm^2, and with $f_1 = 3.1$ mm and $f_2 = 100.1$ mm, the parameters reported in Tab. 2 are obtained.

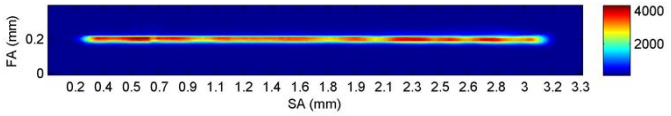

Fig. 8. Example of near-field image.

B. Far-field Measurements

The far-field is measured using the setup illustrated in Fig. 9. The setup is almost the same as that used to measure the near-field, except for replacing the F1 lens with a larger EFL lens and inserting the F3 lens, an achromatic doublet, between the F2 lens and the CCD camera.

From the far-field measurement the divergences θ along the two axes can be calculated as

$$\theta = \frac{f_2}{f_1 f_3} \frac{d_{\text{mea}}}{2}, \tag{21}$$

Table 2. Characteristic parameters computed from near-field measurements.

Parameter	Value
FA Emitter Width @ $1/e^2$ intensity (µm)	1.6
SA Emitter Width @ $1/e^2$ intensity (µm)	93.3

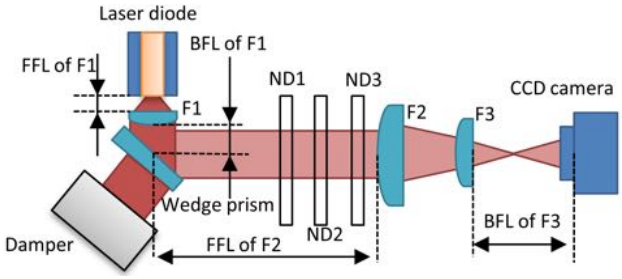

Fig. 9. Far-field measurement setup.

where f_3 is the EFL of F3 and the other symbols have the meaning already introduced.

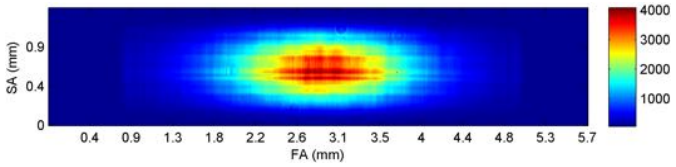

Fig. 10. Example of the far-field image.

The obtained far-field pattern for the considered diode is shown in Fig. 10. From this image and with the help of Eq. 21, with $f_1 = 8$ mm, $f_2 = 100.1$ mm and $f_3 = 49.8$ mm , the parameters reported in Tab. 3 are obtained.

C. Laser Diode Stack Measurement Approach

In our experimental case (and probably this it true also for commercial multi-emitters) we have a single focusing lens, so $f_{\text{foc}_{\text{FA}}} = f_{\text{foc}_{\text{SA}}}$. In order to evaluate the stacking of diode chips all having the same characteristics, we used the approach sketched in Fig. 11 to mimic the actual multi-emitter configuration starting from just the single diode previously characterized. The approach can be divided into 7 steps:

1. Fix the FAC in its nominal position.
2. Adjust the SAC and the laser diode until the beam is well collimated.
3. Change the position of the focusing lens so that the focal plane locates on the CCD exactly.
4. Move the CCD camera (which is mounted on a sub-micrometric 3-axis micro-positioner) along the edge of the staircase defining the spatial stacking up to the position of the n-th diode chip and shoot at the beginning of each step to acquire the image of in the focal plane.
5. Remove the focusing lens and move the CCD camera to the position of the front surface of the focusing lens and shoot to acquire the image of the n-th diode chip at the entrance of the focusing lens.

Table 3. Characteristic parameters computed from far-field measurements.

Parameter	Value
FA divergence @ $1/e^2$ intensity (deg)	22.8
SA divergence @ $1/e^2$ intensity (deg)	6.6

6. Repeat 4th and 5th steps for the desired number of chips to be combined.
7. Combine all the images into two images using a data processing software (Matlab^{TM} in our case): one image is for the beam at the entrance of the focusing lens and the other for the spot at the focal plane.
8. Calculate the characteristic parameters of the combined beam using an approach similar to that previously used for the analysis of the single images.

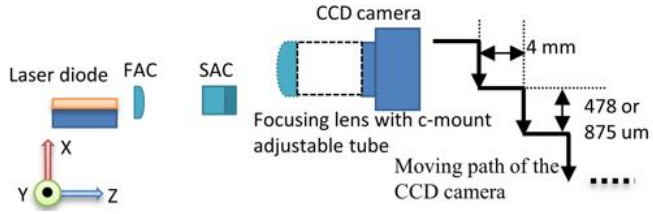

Fig. 11. Approach to emulate the stacking a plurality of diode laser chips by using a single laser diode.

D. Collimated Beam Radius Measurement Results

First the impact of the FAC focal length has been analyzed. The comparison of the results obtained combining 6 chips with two different FAC lenses, namely one with EFL = 600 µm and EFL = 1100 µm is shown in Fig. 12.

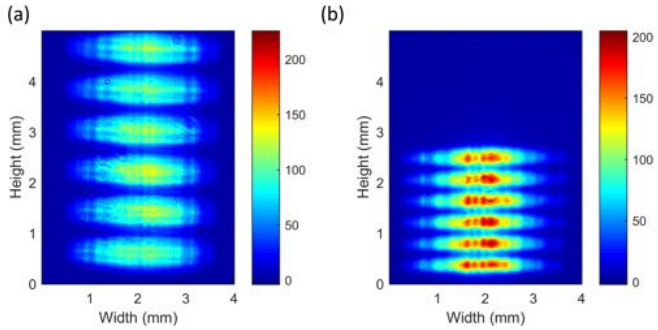

Fig. 12. Comparison of the images at the entrance of the focusing lens for the combination of 6 chips: (a)1100 µm FAC, and (b) 600 µm FAC.

Using the shorter focal length FAC it is possible to further increase the number of combined chips for a fixed aperture: Fig. 13 shows an example with 10 chips; however, decreasing the size of the beam means increasing the divergence of the beam. Furthermore, the closer a laser diode to the CCD camera, the smaller its beam size. Therefore, it is obvious that in Fig. 12 the top beam shape is nearly identical to the bottom beam shape for case (a), while the beams exhibit some degradations for case (b).

Table 4. Comparison between measurements and calculations for the parameters defining the combined beams obtained using different FAC focal lengths.

Item	Measurement	Calculation	Difference
Beam FA width[a] (µm)	5271.2	5253.0	0.3%
Beam SA width[a] (µm)	2706.0	2764.6	2.1%
Beam FA width[b] (µm)	2899.6	2865.0	1.2%
Beam SA width[b] (µm)	2789.6	2764.6	0.9%
Beam FA width[c] (µm)	4800.4	4775.0	0.5%
Beam SA width[c] (µm)	2820.4	2764.6	2.0%

[a]Six combined beams with FAC of EFL 1100 µm. [b]Six combined beams with FAC of EFL 600 µm. [c]Ten combined beams with FAC of EFL 600 µm.

Tab. 4 reports measurements and calculations for the parameters defining the combined beams obtained using different FAC focal lengths and demonstrates the excellent agreement between the two sets.

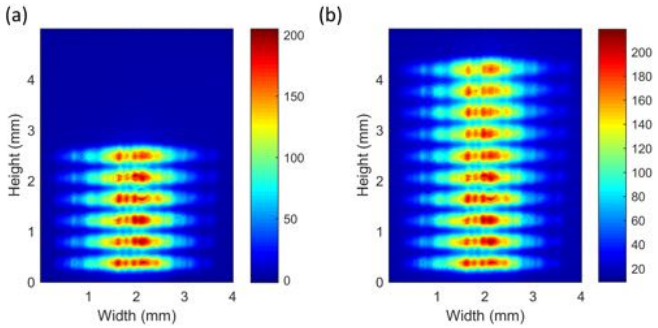

Fig. 13. Comparison of the images at the entrance of the focusing lens using a 600 µm FAC: (a) combination of 6 chips and (b) combination of 10 chips.

E. Focused Beam Measurement Results

An example of the impact of different focusing lenses is shown in Fig. 14, where we compare three lenses, respectively with EFL = 100.1 mm, EFL = 49.8 mm and EFL = 8 mm. The measurements indicate that the spot shrinks when the EFL of the focusing lens decreases.

The experimental results are compared with theoretical predictions in Tab. 5 and Tab. 6 for the stacking of 10 and 6 laser diodes, respectively. Tab. 4 shows that both the number of laser diodes and the EFL of collimator have an impact on the total beam width. If the number of laser diodes or the EFL of collimator increases, the total beam expands. The result in Fig. 14 and in Tab. 7 demonstrate that the focusing spot at focal plane is the same for both the 10 and the 6 diode cases.

F. Error Analysis

The discrepancies between measurements and calculations are quite small, limited to few percents (typically below 5%, except

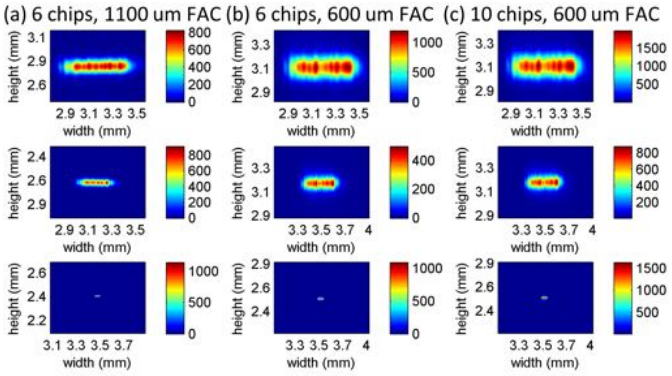

Fig. 14. Visual comparison of the impact of the focusing lens for the combination beams using different FACs and 12 000 µm SAC. The first row is for a focusing lens with EFL = 100.1 mm, the second for a lens with EFL = 49.8 mm and the third for a lens with EFL = 8 mm.

Table 5. Comparison between measurements and calculations for 6 combined beams using a 1100 µm FAC.

Item	Measurement	Calculation	Difference
Spot FA width[a] (µm)	154.0	145.4	5.9%
Spot SA width[a] (µm)	726.0	777.5	6.6%
BPP[a] (mm mrad)	11.0	11.7	6.1%
Spot FA width[b] (µm)	79.2	72.7	8.9%
Spot SA width[b] (µm)	376.2	388.7	3.2%
BPP[b] (mm mrad)	11.4	11.7	2.6%
Spot FA width[c] (µm)	13.2	11.6	13.8%
Spot SA width[c] (µm)	61.6	62.2	1.0%
BPP[c] (mm mrad)	11.7	11.7	0.3%

[a]Focusing lens of EFL = 100.1 mm. [b]Focusing lens of EFL = 49.8 mm. [c]Focusing lens of EFL = 8 mm.

for a single case of 13.8%) as reported in the previous tables, therefore validating the modeling of the multi-emitter system. However, these differences could be even made smaller by acting on the following sources of inaccuracy.

1. Mechanical stability. Despite we used sub-micrometric positioners (with few hundreds of nanometers of accuracy) to control the rotation and the movement of the laser chip and of the SAC, we noticed a transient settling time before which the measurements were continuously changing indicating that the final position assumed by the components might be slightly different from that imposed by the control system. This is clearly a limitation of our system and thus the impact of this component to the total error can be reduced with the help of better positioners.

2. Camera resolution. The resolution of the vision system we used in our setup is 4.4 µm, a value that has negligible impact in the evaluation of large widths (for measurement of quantities larger than 440 µm the contribution to the error is less than 1%), but very relevant in those in the order of tens of micrometers. For example, the error in the measured Spot FA width for a focusing lens with EFL = 8 mm in Tab. 5 is dominated by this contribution since the predicted (calculated) value of 11.6 µm corresponds to 3 camera pixels only. Fitting may help in slightly reducing the impact of this discretization, but the resolution value we have means that, ideally, any actual width between 8.8 µm (2 pixels) and 13.2 µm (3 pixels) always returns 13.2 µm from the camera measurements, with a corresponding error ranging from 0% to 50%. On the other hand, for the largest quantity (as the Beam SA width of 5253 µm for an FAC with EFL = 1100 µm in Tab. 4), the camera contribution to the error is below 0.1% (0.08% in the considered example).

Table 6. Comparison between measurements and calculations for 6 combined beams using a 600 µm FAC.

Item	Measurement	Calculation	Difference
Spot FA width[a] (µm)	277.2	266.7	3.9%
Spot SA width[a] (µm)	734.8	777.5	5.5%
BPP[a] (mm mrad)	7.9	8.2	3.8%
Spot FA width[b] (µm)	140.8	133.3	5.6%
Spot SA width[b] (µm)	374.0	388.8	3.8%
BPP[b] (mm mrad)	8.1	8.2	1.6%
Spot FA width[c] (µm)	22.0	21.3	3.3%
Spot SA width[c] (µm)	61.6	62.2	1.0%
BPP[c] (mm mrad)	8.2	8.2	0.3%

[a]Focusing lens of EFL = 100.1 mm. [b]Focusing lens of EFL = 49.8 mm. [c]Focusing lens of EFL = 8 mm.

3. Focal shift. Since the distance between the collimating lens and the focusing lens is not equal to the sum of the EFLs of two lenses, a focal shift exists; this shift tends to enlarge the spot size at the focal plane, as schematically shown in Fig. 15. This error, however, in our setup becomes relevant only if using a camera with higher resolution since its contribution is currently practically masked by that due to vision system resolution previously discussed. Indeed, the largest influence among the considered lens combination is for the 1100 µm FAC and EFL = 8 mm focusing lens: for the minimum distance between the collimator and the focusing lens of about 50 mm (this distance is practically limited by the thickness of the wedge prism used to route the beam and the neutral density filters that attenuate it not to saturate the camera) the focal shift is 7.5 µm and the spot size increases from 11.6 µm (ideal, without focal shift) to 11.8 µm (imperfect, taking into account of focal shift). The corresponding error would be 1.7%, but this is well below the contribution originated from the vision system. The configuration most tolerant to focal shift is the combination of 600 µm FAC and EFL = 100 mm focusing lens; in this case the spot FA width rises from 266.7 µm to 266.8 µm, with an error below 0.1%.

4. Collimated beam divergence. Due to the divergence of the

Table 7. Comparison between measurements and calculations for 10 combined beams using a 600 µm FAC.

Item	Measurement	Calculation	Difference
Spot FA width[a] (µm)	277.2	266.7	3.9%
Spot SA width[a] (µm)	734.8	777.5	5.5%
BPP[a] (mm mrad)	10.9	11.3	3.4%
Spot FA width[b] (µm)	140.8	133.3	5.6%
Spot SA width[b] (µm)	374.0	388.8	3.8%
BPP[b] (mm mrad)	11.2	11.3	1.2%
Spot FA width[c] (µm)	22.0	21.3	3.3%
Spot SA width[c] (µm)	61.6	62.2	1.0%
BPP[c] (mm mrad)	11.4	11.3	0.7%

[a]Focusing lens of EFL = 100.1 mm. [b]Focusing lens of EFL = 49.8 mm. [c]Focusing lens of EFL = 8 mm.

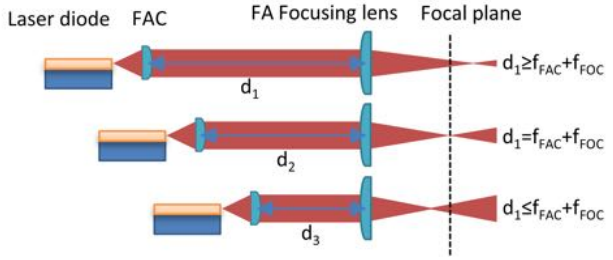

Fig. 15. Schematic representation of the spot size enlargement at the focal plane caused by the focal shift.

collimated beam (albeit small), the beam width expands as the distance between the focusing lens and the laser diode increases. So the beam width is larger than the waist width before propagating though the focusing lens, which leads to smaller spot size. As said, this effect is not taken into account in current model.

5. CONCLUSION

A model to predict the BPP of a stack of incoherent beams has been developed. The model considers the impact of collimating and focusing lenses and can be used to choose for their optimal values to maximize the brilliance of the beam coupled to an output fiber. The theoretical predictions have been validated in a simplified experimental setup, where a beam stack have been mimicked by using a single emitter and moving the focusing lens. Then, the model has been applied to study the configuration of a typical multi-emitter module and to calculate the maximum number of diodes that can be coupled into a delivery fiber with given core diameter and numerical aperture.

Funding. H.Y. acknowledges the sponsorship of the China Scholarship Council (CSC).

REFERENCES

1. K. Price, F. Pfeffer, P. Leisher, S. Karlsen, and R. Martinsen, "KW-class industrial diode lasers comprised of single emitters," in "Proc. SPIE," , vol. 7583 (2010), vol. 7583.
2. B. Koehler, A. Segref, P. Wolf, A. Unger, H. Kissel, and J. Biesenbach, "Multi-kW high brightness fiber coupled diode laser," in "Proc. SPIE," , vol. 8605 (2013), vol. 8605.
3. S. Strohmaier, C. Tillkorn, P. Olschowsky, and J. Hostetler, "High-power, high-brightness direct-diode lasers," Optics and Photonics News **21**, 24–29 (2010).
4. A. Braglia, A. Califano, Y. Liu, M. Olivero, G. Perrone, and R. Orta, "Devices and pumping architectures for 2¯m high power fiber lasers," in "Proc. SPIE," , vol. 9135 (2014), vol. 9135.
5. A. Braglia, A. Califano, Y. Liu, and G. Perrone, "Architectures and components for high power cw fiber lasers," International Journal of Modern Physics B **28**, 1–14 (2014).
6. S. R. Karlsen, R. K. Price, M. Reynolds, A. Brown, R. Mehl, S. Patterson, and R. J. Martinsen, "100-W 105-¯m 0.15 NA fiber coupled laser diode module," in "Proc. SPIE," , vol. 7198 (2009), vol. 7198.
7. E. Rodríguez-Vidal, I. Quintana, J. Etxarri, U. Azkorbebeitia, D. Otaduy, F. González, and F. Moreno, "Optical design and development of a fiber coupled high-power diode laser system for laser transmission welding of plastics," Optical Engineering **51**, 124301–124301 (2012).
8. Z. Wang, S. Drovs, A. Segref, T. Koenning, and R. Pandey, "Fiber coupled diode laser beam parameter product calculation and rules for optimized design," in "Proc. SPIE," , vol. 7918 (2011), vol. 7918.
9. H. Sun, *Laser diode beam basics, manipulations and characterizations* (Springer Science & Business Media, 2012).
10. C. NelsoN and J. Crist, "Predicting laser beam characteristics," Laser Technik Journal **9**, 36–39 (2012).
11. II-VI Laser Enterprise Laser Diodes Data Sheet, "9w 9xx nm 90um high power single emitter laser diode on c-mount," http://www.laserenterprise.com/resources/pdf/high-power-laser-diodes/ohse/D00466-PB_SEC9-9xx-01_Datasheet_Iss01.pdf ((downloaded 03/2015)).